JOURNAL OF GEOPHYSICAL RESEARCH, VOL. 100, NO. D12, PAGES 26,117–26,134, DECEMBER 20, 1995

General circulation model assessment of the sensitivity of direct climate forcing by anthropogenic sulfate aerosols to aerosol size and chemistry

Olivier Boucher

Laboratoire de Météorologie Dynamique du CNRS, Ecole Normale Supérieure, Paris, France

Theodore L. Anderson

Department of Atmospheric Sciences, University of Washington, Seattle

Abstract. Climate response to atmospheric changes brought about by human activity may depend strongly on the geographical and temporal pattern of radiative forcing [*Taylor and Penner*, 1994]. In the case of aerosols stemming from anthropogenic sulfur emissions, geographical and temporal variations are certainly caused by variations in local mass concentration [*Charlson et al.*, 1991; *Kiehl and Briegleb*, 1993], but could also arise from variations in the optical properties of sulfate aerosols. Since optical properties (including their relative humidity (RH) variation) depend fundamentally on aerosol size and chemical form and since size and chemical form are features of the aerosol which are not likely to be modeled on the global scale in the near future, geographical and temporal variations in optical properties could represent a stumbling block to accurate climate change forecasts. While extensive measurements of aerosol optical properties are needed to fully assess this problem, a preliminary assessment can be gained by considering the sensitivity of climate forcing to realistic variations in sulfate aerosol size and chemical form. Within a plausible set of assumptions (sulfate aerosol resides in the accumulation mode size range and only interacts with water vapor and ammonia vapor), we show that this sensitivity is fairly small (±20%). This low sensitivity derives from a number of compensating factors linking the three optical parameters identified by *Charlson et al.* [1991]. By implication, these optical parameters, low RH scattering efficiency, the ratio of hemispheric backscatter to total scatter, and the RH dependence of scattering efficiency, should not be treated independently in either theoretical or experimental investigations of direct climate forcing. A suggested logical focus for such investigations is the backscatter efficiency at high RH. If borne out by future research, low sensitivity to sulfate aerosol size and chemistry would mean that direct sulfate climate forcing can be incorporated in global climate models with only a knowledge of sulfate mass concentration. We emphasize, therefore, the need to study the extent to which our assumptions break down, in particular, the fraction of anthropogenic sulfate that forms on coarse mode particles (i.e., those with diameters > 1 μm) and the extent and effects of sulfate interactions with other accumulation mode components. Finally, we find that a significant fraction of direct aerosol forcing occurs in cloud-covered regions, according to a simple bulk parameterization.

1. Introduction

The ability of atmospheric aerosols to affect the radiative balance of the Earth has been recognized for several decades both regarding their direct effect on backscattering of sunlight [*McCormick and Ludwig*, 1967; *Charlson and Pilat*, 1969; *Atwater*, 1970; *Rasool and Schneider*, 1971] and their indirect effect (also referred to as the "Twomey" effect), whereby cloud optical properties are influenced by the available number concentration of cloud condensation nuclei [*Twomey*, 1974, 1977; *Twomey et al.*, 1984]. *Bolin and Charlson* [1976] estimated the direct forcing of anthropogenic sulfate particles in terms of a temperature decrease of -0.03 to -0.06 K but they significantly underestimated the surface area of the Earth affected by anthropogenic sulfate aerosols. The first attempts to incorporate an aerosol

Paper number 95JD02531.
0148-0227/95/95JD-02531$05.00

climatology in a global model are due to *Toon and Pollack* [1976] and *Coakley et al.* [1983]. The latter showed that "background aerosols", which were largely sulfates, could cool the Earth's surface by 2 to 3 degrees. When it was realized that the sulfur cycle, at least in the northern hemisphere, was dominated by anthropogenic emissions [*Langner et al.*, 1992], it became undoubted that anthropogenic sulfate particles have a non-negligible effect on the Earth's radiative balance.

Using the global distribution of anthropogenic sulfate aerosol derived by *Langner and Rodhe* [1991] [see also, *Langner et al.*, 1992], *Charlson et al.* [1991] (hereafter C91) re-estimated the direct climate forcing stemming from anthropogenic SO_2 emissions. They showed that this forcing, while highly uncertain, is significant in magnitude when scaled against present-day forcing by anthropogenic greenhouse gases. By implication, accurate climate change forecasts would be impossible until the climate forcings due to anthropogenic aerosols were included. Successive studies have confirmed this point. *Kiehl and Briegleb* [1993] (hereafter KB93) showed that the geographical pattern of climate forcing changes dramatically when anthropogenic sulfate aerosols are included, while *Taylor and Penner* [1994] showed that both the pattern of climate response and the globally averaged climate sensitivity are highly dependent upon the geographical pattern of forcing. Though not explicitly stated, these conclusions apply to the temporal pattern of climate forcing as well, which is markedly variable for aerosols on diurnal, synoptic, and seasonal scales.

Using a "reference box model", *Charlson et al.* [1991, 1992] systematized the climate forcing calculation into a set of nine key parameters (see Table 1 by *Charlson et al.* [1992]). These parameters can be divided into three categories: (1) parameters for predicting the mass concentration of anthropogenic sulfate, (2) parameters for predicting the optical properties of anthropogenic sulfate with respect to the scattering of solar radiation, and (3) parameters for predicting the incident flux of solar radiation. There is a long history of model development with respect to category 3, which includes such parameters as solar zenith angle, surface albedo, and the global distribution and radiative properties of gases and clouds in the atmosphere. Models have also been developed [*Langner and Rodhe*, 1991; *Langner et al.*, 1992; *Taylor and Penner*, 1994] with respect to category 1, as stated above. Though considerable refinement of these models is required, it is already clear that they produce reasonable results when compared to observations [*Langner et al.*, 1993]. Category 2, the optical properties of sulfate aerosols (including their dependence on ambient relative humidity), presents a major potential difficulty.

Climate forcing estimates to date [C91; KB93; *Taylor and Penner*, 1994] differ by a factor of 3, mostly attributable to different assumptions about optical properties. These optical properties depend fundamentally on the size and chemical form of the sulfate aerosol particles, yet models predicting aerosol size and chemical form on a global scale are not currently available nor are they likely to be developed in the near future. Therefore the accuracy of climate forcing estimates, and in particular the spatial and temporal pattern of this forcing, is likely to be limited for some time to come by the spatial and temporal variability of climatically relevant aerosol optical properties, what could be termed the "climate forcing efficiency" (per unit mass) of an aerosol component. By using existing models for categories 1 and 3 above and by adopting a plausible set of simplifying assumptions, this article will explore possible variations in the climate forcing efficiency of sulfate aerosols.

Within category 2, C91 identified three parameters that must be considered in order to predict the radiative effect of sulfate aerosol from the sulfate mass concentration. These are the light scattering efficiency per unit sulfate mass at low relative humidity (RH), $\alpha_{sp-SO_4^=}$, the fraction of scattered light which is scattered into the backward hemisphere, b (closely related to the asymmetry parameter, g, used by two-stream radiative transfer calculations), and the increase in light scattering as a function of relative humidity, f(RH), which results from the hygroscopic nature of sulfate aerosols. Each of these parameters exhibits strong variations with particle size, wavelength, and chemical form, and these variations are not independent. For instance, KB93 pointed out based on Mie calculations with various size distributions of sulfuric acid aerosol that increases in $\alpha_{sp-SO_4^=}$ are associated with decreases in b. (For solar wavelengths, this result applies to particle sizes in the accumulation mode: $0.1 < D_p < 1$ μm.) This is a compensating effect. That is, the climate forcing efficiency of accumulation mode sulfate aerosols is seen to be much less sensitive to particle size when the interdependence of $\alpha_{sp-SO_4^=}$ and b is taken into account than when the two are considered separately. Because f(RH) also varies with particle size [*Hegg et al.*, 1993], the interdependence extends to this parameter as well. However, KB93 were not able to consider this because they adopted f(RH) from empirical studies [*Charlson et al.*, 1984] as a single, unvarying function. Moreover, KB93 did not treat the RH dependence of g.

Our study attempts to incorporate all these interrelationships. To do this requires knowledge of the low RH size distribution and of the RH variations of particle size, density, and refractive index for each chemical form. Given this knowledge, all optical properties required for incorporating sulfate aerosols into the radiative transfer portion of the general circulation model (GCM) can be calculated from Mie theory. We assume (1) that anthropogenic sulfate mass resides in the accumulation mode and (2) that sulfate aerosol only interacts with gas phase ammonia and/or water vapor. The first assumption restricts particle size to within the range of measurements for the accumulation mode. The second assumption restricts the sulfate aerosol chemical form to the ammonium–sulfate–water system, for which extensive laboratory data on hydration behavior is available. In essence, our assumptions constitute a simple but plausible physical–chemical model of sulfate aerosol which allows the interdependence of $\alpha_{sp-SO_4^=}$, b, and f(RH) to be explored via their mutual dependence on particle size, wavelength, and chemical form.

We use sulfate mass concentrations (category 1 above) from *Langner and Rodhe* [1991], as in previous climate forcing calculations [C91, KB93]. Climate forcing, which depends among other factors on the temporal and spatial distributions of RH, clouds, surface albedo, and solar zenith angle, is calculated with the Laboratoire de Météorologie Dynamique (LMD) GCM. Three chemical forms are tested with ammonium-to-sulfate ratios of 2 (ammonium sulfate), 1 (ammonium bisulfate), and 0 (sulfuric acid). For ammonium sulfate we test the effect of hysteresis in the growth curve between 40 and 80% RH. In addition, we test size distributions centered at 0.15, 0.20, 0.30, 0.40, and 0.60 μm (dry aerosol geometric volume mean diameter, D_{gv0}). (The extreme sizes are outside the range of most observations for accumulation mode aerosols, but are included to show size dependent tendencies.) Optical properties for each aerosol type are calculated according to Mie theory at 12 values of RH and for 24 wavelengths. The wavelength information is then compressed into the two wavebands available in the LMD GCM by taking weighted averages over the solar power spectrum. We test the influence of this averaging procedure by considering both top-of-atmosphere and bottom-of-atmosphere solar spectra (the latter calculated for clear sky midlatitude summer conditions). We use the GCM to calculate climate forcings only, not climate effects or feedbacks between the climate system and the sulfate aerosol. Details of the calculations are given in the next section.

2. Brief Description of the Models

2.1. The MOGUNTIA Model

The MOGUNTIA model was initially developed by Zimmermann [*Zimmermann*, 1984; 1987] at University of Mainz, Germany. It is an Eulerian transport model, with a 10° resolution in latitude and longitude and 10 vertical layers. Wind, precipitation, and temperature are prescribed from climatological monthly values. This model has been used at Department of Meteorology, Stockholm University, to describe the tropospheric sulfur cycle [*Langner and Rodhe*, 1991]. Three sulfur components are considered: dimethylsulfide (DMS), sulfur dioxide (SO_2), and aerosol sulfate ($SO_4^=$). Sources are divided into anthropogenic and natural emissions as shown in Table 1. We consider in this study that 90% of the biomass burning SO_2 emissions are anthropogenic. The model (in its "standard oxidation" version) was run twice, a first time with natural sources only (preindustrial case), the second time with natural and anthropogenic sources (industrial case). Monthly mean values of the aerosol mass fields are extracted from the last 12 months of 18 month integrations. The model has been compared to different sets of measurements [*Langner and Rodhe*, 1991; *Langner et al.*, 1993]. In general, there is a fair agreement between modeled sulfate concentration and observations. However, the model has to be improved regarding the treatment of chemical processes and the estimates of the sources in order to better simulate the seasonal variability. The geographic distribution of annually averaged sulfate burden in both integrations (preindustrial and industrial cases) are displayed in Figure 1. The burden of anthropogenic sulfate, obtained by difference, is given in Table 2 for each hemisphere and each of the two specific regions considered.

Table 1. Emission Rates of Sulfur Components Used in the Model Calculations

Sources	Industrial Case	Preindustrial Case
Anthropogenic SO_2	66.5	0
Anthropogenic $SO_4^=$	3.5	0
Biomass burning (SO_2)	2.5	0.25
Volcanoes (SO_2 + $SO_4^=$)	8.5	8.5
Oceans (DMS)	16	16
Soils and plants (DMS)	1	1

Emission rates are in teragrams sulfur per year. DMS is dimethylsulfide.

2.2. The LMD GCM

The LMD GCM is a grid point model that has been developed for climate studies. It has been initially described by *Sadourny and Laval* [1984] and *Le Treut and Li* [1991]. The resolution is 64 points evenly spaced in longitude, 50 points evenly spaced in sine of the latitude and 11 σ-levels. The radiative parameterization is an improved version of the codes described by *Fouquart and Bonnel* [1980] (solar radiation) and *Morcrette* [1991] (terrestrial radiation) and is the same as the one implemented in the model of the European Centre for Medium-Range Weather Forecasts (ECMWF). The technical points of the scheme (including the treatment of aerosols) are best documented by *Morcrette* [1989]. The shortwave spectrum is divided into two spectral intervals: 0.25–0.68 and 0.68–4.00 μm. The radiation routine is called every 2 hours. The model accounts for the diurnal cycle of solar radiation and allows fractional cloudiness to form in a grid box. In the cloud-filled portion of a grid box, the optical properties (τ, ω, and g) of gases, aerosol particles, and cloud droplets are combined and the Delta-Eddington assumption is made. In the cloud-free portion of a grid box, the optical properties of gases and aerosols are combined and a Delta approximation of the forward scattering peak is made to account for the highly asymmetric aerosol phase function. The reflectivity and the transmissivity of a layer are simply the average of the clear and cloudy sky reflectivities and transmissivities weighted linearly by their respective fractions in the layer. This is equivalent to the random overlap assumption [*Morcrette and Fouquart*, 1986].

We predict cloud cover from a simple statistical scheme where total water (water vapor and cloud water) is assumed to be uniformly distributed in a grid box [*Le Treut and Li*, 1991]. The cloud fraction is defined as the part of the grid box where the total water exceeds

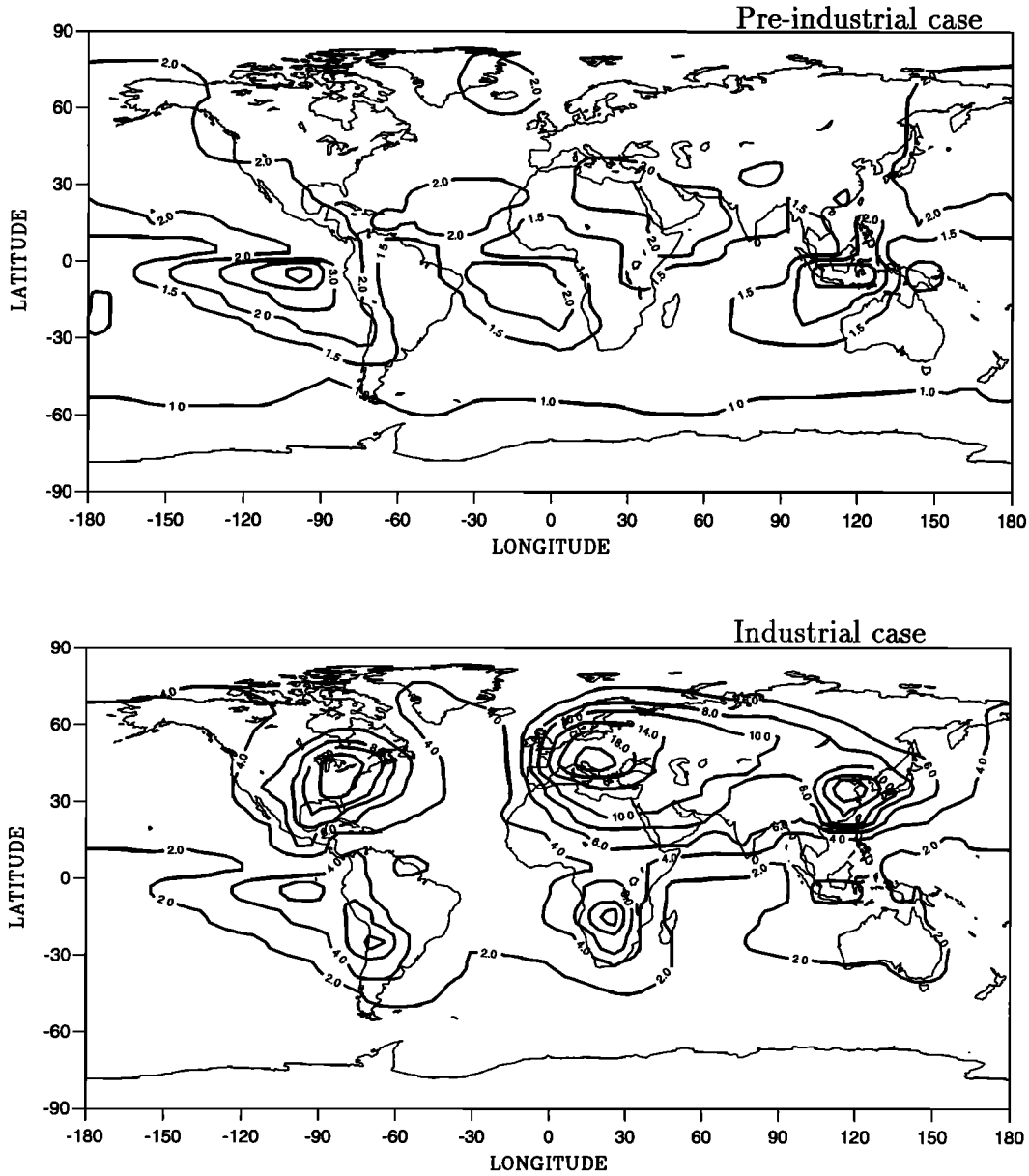

Figure 1. Sulfate aerosol burdens (milligrams of sulfate per square meter) in the preindustrial and industrial cases as simulated by the MOGUNTIA model (see *Langner and Rodhe* [1991] and *Langner et al.* [1992]).

the water vapor mixing ratio at saturation. Part of the water is condensed in the cloudy part and liquid water content is predicted. Water vapor mixing ratio is computed both in the clear sky and the cloudy part of the grid box. The clear sky relative humidity is then stored for use in the aerosol parameterization. The prescribed sulfate aerosol vertical distribution in the GCM is the same as the one simulated by the chemical model and the grid change is made in such a way that the total sulfate aerosol burden is kept the same.

The shortwave radiative fluxes are computed at each time step for each aerosol type, with and without the presence of clouds and with and without the influence of relative humidity on aerosol growth. To advance from one time step to the next, preindustrial sulfate concentrations are used. Thus we do not consider feedbacks between anthropogenic sulfate aerosol and the climate system.

The model is run for 1 year. While its output does not, therefore, represent a climatology, it is useful to examine the cloud and RH fields for reasonableness. The simulated "cloud radiative forcing" is in good agreement with the Earth Radiation Budget Experiment (ERBE) data [*Ramanathan et al.*, 1989]. The seasonal cycle is well reproduced, although the simulated forcing is too small in the midlatitudes of the southern hemisphere (SH) summer and is too high in the tropics. Cloud cover (CC) is computed every half-hour and is averaged temporally assuming a random overlap in the vertical. The random overlap hypothesis is reasonable here con-

sidering the roughness of the vertical resolution and is consistent with the treatment of fractional cloudiness in the parameterization of radiation. The annually averaged value of CC is 49.7, 55.4, and 52.6% for the NH, SH, and globe, respectively (Table 2a). These values are somewhat lower than the climatological averages from satellite- and ground-based estimates [*Mokhov and Schlesinger*, 1994]. Clear sky daytime relative humidity ranges from 20 to about 80%. Averaged in lower 2 km, it is higher over ocean (67.1%) than over land (57.5%) (see Table 2a). Relative humidity is about 73 and 55% in the first vertical layer (~980 hPa) over ocean and land, respectively. It is relatively constant with height within the boundary layer, while it decreases above the boundary layer.

3. Sulfate Aerosol Optical Properties

The shortwave radiative transfer portion of the LMD GCM requires the knowledge of vertical aerosol optical depth, τ_p, single scattering albedo, ω, and asymmetry parameter, g. Because hydrated sulfuric acid and hydrated ammonium-sulfate salts are essentially nonabsorbing at wavelengths below 2 μm [*Kent et al.*, 1983] and because the small fraction of solar power above 2 μm (<5%) is mostly absorbed by atmospheric gases, we set $\omega = 1$. This implies that $\tau_p = \tau_{sp}$, where τ_{sp} is the vertical optical depth due to scattering by particles and depends on both the concentration of the sulfate aerosol and its optical properties:

$$\tau_{sp} = \sigma_{sp}\,\Delta z = \alpha_{sp-SO_4^=}\, m_{SO_4^=}\,\Delta z \qquad (1)$$

Here σ_{sp} is the aerosol scattering coefficient (per meter), Δz is the vertical thickness (meters) of the GCM grid box, and $m_{SO_4^=}$ is the sulfate ion mass concentration (grams per cubic meter) as predicted by the *Langner and Rodhe* [1991] model. Equation (1) defines $\alpha_{sp-SO_4^=}$, the sulfate scattering efficiency (with unit meters squared per gram). Note that this quantity trans-

Table 2a. Climatic Parameters from Global Models: Global Scale Parameters

	NH	SH	Globe
ASCB (Anthropogenic Sulfate Column Burden (mg $SO_4^=$ m^{-2})*)*			
Ocean	2.20	0.59	1.28
Land	6.16	2.09	4.83
Combined	3.76	0.88	2.32
C91	3.58	0.41	2.00
KB93	2.93*	0.60*	1.77*
RH low (Clear Sky Daytime RH in Lower 2 km)			
Ocean	66.9%	67.2%	67.1%
Land	56.0%	60.5%	57.5%
Combined	62.6%	65.9%	64.3%
CC (Cloud Cover)			
Ocean	55.0%	56.7%	56.0%
Land	41.6%	50.0%	44.3%
Combined	49.7%	55.4%	52.6%
C91			61%
KB93			62%
CFE (Climate Forcing Efficiency (W (g $SO_4^=$)$^{-1}$)*)*			
Ocean	−137	−135	−136
Land	−118	−120	−118
Combined	−125	−128	−125
C91	−299	−268	−300
KB93	−147	−217	−158
RH-factor			
Ocean	1.49	1.36	1.45
Land	1.37	1.28	1.36
Combined	1.41	1.33	1.40
Cloud-factor			
Ocean	0.55	0.56	0.56
Land	0.64	0.71	0.65
Combined	0.60	0.62	0.61
C91			0.39
KB93			0.64*

* B. Briegleb, personal communication, 1994.

Table 2b. Climatic Parameters from Global Models: Regional Parameters

	Eastern United, States, January	Eastern United States, July	Europe, January	Europe, July
ASCB	15.8	12.7	22.7	20.1
RH low	64.4%	68.6%	74.3%	59.9%
CC	82.2%	70.5%	71.6%	28.1%
CFE	−80	−132	−62	−193
RH factor	1.53	1.64	1.87	1.41
Cloud factor	0.34	0.46	0.28	0.72

Average values of key prognostic variables are from the global-scale models MOGUNTIA and the LMD GCM. Variable definitions are given in Table 2a for use in part Table 2b.

Table 2a gives averages over the northern hemisphere (NH), southern hemisphere (SH), and globe, separated in each case into ocean, land, and combined. Additional rows indicate the values, where known, from the studies of C91 and KB93.

Table 2b gives the averages over two specific, high-concentration regions for two specific months of the year. (See Figure 5 for further information on this regional study.)

forms the mass concentration of sulfate anion into light scattering by the complete, sulfate-containing, aerosol component, which can include, depending on chemical form and ambient RH, ammonium cations and/or water of hydration. The RH dependent values of $\alpha_{sp-SO_4^=}$ are derived from standard Mie calculations [*Bohren and Huffman*, 1983] as follows.

Assuming internally homogeneous spheres (nonabsorbing in our case), Mie theory predicts the scattering cross section, A_{sp}, of individual particles as a function of their diameter, D, real refractive index, n, and the wavelength of incident light, λ. Because particle volume, V_p, depends only on D (for spheres), a straightforward application of Mie theory is to calculate the volume scattering efficiency of a lognormal particle size distribution,

$$\alpha_{sp-V} = \frac{A_{sp}(D_{gv}, \sigma_g, n, \lambda)}{V_p}, \qquad (2)$$

where D_{gv} and σ_g are the geometric volume mean diameter and geometric standard deviation, respectively, and V_p and A_{sp} now represent integrations over the particle size distribution. Converting α_{sp-V} to mass scattering efficiency would require additional information about the ratio of particulate mass to volume. Similarly, for pure sulfate particles (i.e., composed only of sulfate ions and chemically associated water, hydrogen ions and/or ammonium ions), α_{sp-V} can be converted to $\alpha_{sp-SO_4^=}$ given the ratio of sulfate ion mass to particulate volume:

$$\alpha_{sp-SO_4^=} = \alpha_{sp-V} \frac{V_p}{m_{SO_4^=}} = \frac{\alpha_{sp-V}}{C_{SO_4^=}}, \qquad (3)$$

where $C_{SO_4^=}$ is the particulate phase sulfate ion concentration (grams per cubic centimeter). The hydration dependent quantities in (2)–(3) are D_{gv}, n, V_p, and $C_{SO_4^=}$. The parameterization of their RH dependence is discussed below ((4)–(5) and associated text).

The same, hydration dependent Mie calculations that predict A_{sp} for individual particles also predict the scattering phase function, $P(\Phi)$. Appropriate integrations of $P(\Phi)$ yield both g (the asymmetry parameter or intensity-weighted average of $\cos(\Phi)$) and b (the ratio of hemispheric backscattering to total scattering). Thus hydration effects on both scattering efficiency and the angular distribution of scattered intensity are propagated in a self-consistent manner through all the chemical and physical tests. To calculate g and b for a size distribution, A_{sp}-weighted averages are used. For averages over selected portions of the solar power spectrum, weighting is by both A_{sp} and solar power.

To explore possible variations in sulfate aerosol optical properties, we consider 11 aerosol types. Each aerosol type defines the wavelength and RH dependent values of $\alpha_{sp-SO_4^=}$ and g. We will also present values of the hemispheric backscattering efficiency, $\alpha_{bsp-SO_4^=}$, since this quantity can be related to backscatter measurements by nephelometry [*Charlson et al.*, 1974]. $\alpha_{bsp-SO_4^=}$ is defined like $\alpha_{sp-SO_4^=}$, except that where $\alpha_{sp-SO_4^=}$ represents all scattering angles (0 to 180°), $\alpha_{bsp-SO_4^=}$ represents scattering in the backward hemisphere only (scattering angles of 90 to 180° with respect to the incident ray). The backscatter fraction, b, is defined as the ratio between $\alpha_{bsp-SO_4^=}$ and $\alpha_{sp-SO_4^=}$. The backscatter fraction is not used in our radiative transfer calculation, but is presented for the sake of comparison with previous investigators [*Charlson et al.*, 1991; 1992]. Note that b is equivalent to the "upscatter fraction" (fraction of incident solar radiation scattered upward to space) for a solar zenith angle of 0°. Table 3 summarizes the 11 aerosol types. Using aerosol type A as the reference, we can explore the sensitivity of climate forcing to the hysteresis effect (types A, B, and C), the aerosol size distribution (types D to H), the chemical form (types A, I, and J), and the spectral averaging procedure (types A and K).

Table 3. Aerosol Types

Aerosol Type	Chemical Composition	D_{gv0}, μm	σ	Hydration Growth	Spectral Averaging
		Base Case			
A	$(NH_4)_2SO_4$	0.30	2.0	interp.	BOA
		Hysteresis Tests			
B	$(NH_4)_2SO_4$	0.30	2.0	rising RH	BOA
C	$(NH_4)_2SO_4$	0.30	2.0	falling RH	BOA
		Particle Size Tests			
D*	$(NH_4)_2SO_4$	0.15	1.4	interp.	BOA
E	$(NH_4)_2SO_4$	0.20	1.4	interp.	BOA
F	$(NH_4)_2SO_4$	0.30	1.4	interp.	BOA
G	$(NH_4)_2SO_4$	0.40	1.4	interp.	BOA
H*	$(NH_4)_2SO_4$	0.60	1.4	interp.	BOA
		Chemical Form Tests			
I	$(NH_4)HSO_4$	0.30	2.0	falling RH	BOA
J	H_2SO_4	0.30	2.0	N/A	BOA
		Spectral Averaging Test			
K	$(NH_4)_2SO_4$	0.30	2.0	interp.	TOA

D_{gv0} and σ_g are the geometric volume mean diameter (at 0% RH) and geometric standard deviation defining a lognormal size distribution. The hydration column refers to the hysteresis phenomenon for ammonium sulfate and ammonium bisulfate and tells whether hydration data was taken from the rising RH or the falling RH growth curves or from a curve which interpolates between the two (interp.). Optical properties (see Table 5) are averaged over either the bottom-of-atmosphere (BOA) or top-of-atmosphere (TOA) representation of the solar power spectrum. N/A means "Not applicable".

*Types D and H are unrealistic sizes for accumulation mode aerosols.

The sulfur cycle model of *Langner and Rodhe* [1991] predicts the global distribution of aerosol sulfate derived from anthropogenic sulfur emissions but does not predict the associated cations (usually hydrogen and/or ammonium) nor the amount of chemically held, condensed-phase water. Sulfur emissions are responsible for the presence of these cations and water in the condensed phase since these species would be in the gas phase in the absence of the sulfur emissions. This is certainly the case with water and generally the case with ammonia. (An exception would be sulfuric acid reacting with particulate phase ammonium nitrate to volatilize nitric acid. Because nitrate is a small fraction of aerosol mass outside of selected urban areas [*White*, 1990] and because ammonium nitrate is likely to occur on coarse mode particles that are externally mixed with ammonium sulfates, this reaction is probably of secondary importance.) Because the most likely cations are hydrogen and ammonium and because the ammonium-sulfate-water system is quite well understood, we restrict ourselves to these species.

In essence, then, we are testing the sensitivity of climate forcing by acidic sulfate aerosols to the degree of ammonia neutralization: the ammonium-to-sulfate ratio is varied from 0 (sulfuric acid) to 1 (ammonium bisulfate) and 2 (ammonium sulfate). The degree of neutralization involves a compensating effect. Sulfuric acid particles are extremely hygroscopic and will draw significant water mass into the aerosol phase at any RH. If these particles are partially or completely neutralized by drawing ammonia from the gas phase, there will be an increase in particle mass due to the added ammonium but a decrease in particle hygroscopicity (especially at low RH) and thus a decrease in particulate water mass. Ammonia neutralization also affects particle size and refractive index at each RH.

Table 4 lists the properties of anhydrous sulfate compounds as well as the properties of pure water. Aerosol hydration is predicted based on laboratory studies of single-component aerosols which describe the variation of water activity (equivalent to RH for particles larger than about 0.1 μm diameter) and droplet density, ρ_d, as functions of solute mass fraction, x_{ms}. These results can be used to predict the diameter growth factor, D_d/D_0 (where D_d and D_0 are the volume equivalent diameters of the droplet and dry crystal, respectively), using

$$\frac{D_d}{D_0} = \left(\frac{\rho_0}{\rho_d\, x_{ms}}\right)^{\frac{1}{3}} \tag{4}$$

Here ρ_0 is the density of the anhydrous particle (Table 4). Similarly, the particulate phase concentration of sulfate ion, $C_{SO_4^=}$, for input to (3), can be calculated from

$$C_{SO_4^=} = \rho_d\, x_{ms}\, \frac{M_{SO_4^=}}{M_s}, \tag{5}$$

Table 4. Properties of Water and Anhydrous Sulfate Compounds

Compound	Formula	M_j, g mol^{-1}	ρ_0, g cm^{-3}	$n(0.589)$	R_j, cm^3 mol^{-1}	DH	CH
Water	H_2O	18.02	0.997	1.333[a]	3.1724[b]		
Ammonium sulfate	$(NH_4)_2SO_4$	132.14	1.769[c]	1.521[c]	23.50[d]	80%[d]	37%[d]
Ammonium bisulfate	$(NH_4)HSO_4$	115.11	1.78[c]	1.473[c]	18.38[d]	39%[d]	< 5%[d]
Sulfuric acid	H_2SO_4	98.08	1.841[c]	1.426[b]	13.45[b]	<1%	<1%

M_j is the molecular weight, ρ_0 the density, $n(0.589)$ the real refractive index at 0.589 μm wavelength, and R_j the partial molar refraction of the pure compound. The exception to this is sulfuric acid, where ρ_0 and $n(0.589)$ apply to a 97% pure (by mass) mixture with water. In this case, $n(0.589)$ is calculated using the *Stelson* [1990] method along with the R_j and ρ_0 values given here. DH is the deliquescent relative humidity and CH the crystallization relative humidity for aerosol particles consisting of the given compound plus water.
[a] *Kent et al.* [1983].
[b] *Stelson* [1990].
[c] *Weast* [1987].
[d] *Tang and Munkelwitz* [1994].

where $M_{SO_4^=}$ and M_s are the molar masses (grams per mole) of sulfate ion and the solute, respectively. The real refractive index at 0.589 μm wavelength, $n(0.589)$, is calculated from x_{ms} and the partial molar refraction, R_j, of each species following *Stelson* [1990]. Values of R_j are given in Table 4. There is a small wavelength dependence to refractive index over the solar spectrum which takes a similar form for all the species (water, sulfate, and ammonium) under consideration. Available data [*Kent et al.*, 1983; *Palmer and Williams*, 1975] were closely matched by setting $n(\lambda) = n(0.589) - 0.03\,(\lambda - 0.589)$, where λ is the wavelength in μm.

Most atmospheric aerosol particles, including H_2SO_4, $(NH_4)HSO_4$, and $(NH_4)_2SO_4$ particles are hygroscopic: their physical and optical characteristics are dependent on the relative humidity of the ambient atmosphere. Whereas sulfuric acid particles are always hydrated, ammonium bisulfate and ammonium sulfate particles can exist as dry crystals at sufficiently low RH and experience an abrupt change in size with increasing RH when a specified RH is reached. This RH, called the deliquescence relative humidity (DH), is 80% for $(NH_4)_2SO_4$ [*Tang and Munkelwitz*, 1994; *Shaw and Rood*, 1990; *Covert et al.*, 1972] and 39% for $(NH_4)HSO_4$ [*Tang and Munkelwitz*, 1994]. However, the particle does not behave in the same way for increasing and decreasing RH conditions. When RH decreases, a particle does not crystallize at the DH but remains in a metastable state until the crystallization relative humidity (CH) is reached. This hysteresis phenomenon can be neglected for ammonium bisulfate because the CH (< 5% [*Tang and Munkelwitz*, 1994]) is below normal values encountered in the lower troposphere. That is, we can reasonably assume that ammonium bisulfate particles will always be hydrated. For ammonium sulfate, however, hysteresis occurs over a much more common range of RH values (37 to 80%) such that metastable droplets are much more likely. The existence of metastable droplets for ambient RH within this range has been shown to be a common feature of the atmospheric aerosol at a variety of urban and rural sites [*Rood et al.*, 1989]. *Hänel and Lehmann* [1981] also observed the hysteresis cycle on several samples. This has important implications for the computation of aerosol optical properties since part of the light-scattering is due to the liquid H_2O incorporated in the metastable droplets. The question thus arises whether to follow the rising or falling RH growth curve, which requires a knowledge of the RH history of each air parcel. Lacking such detailed information, we test the sensitivity of climate forcing to hysteresis: both curves are included in these calculations as well as an "average" curve based on a simple linear interpolation of droplet diameter growth between the 40% (no growth) and 80% RH points.

For a given mass concentration, the primary factor affecting the light-scattering efficiency of an aerosol population is its size distribution. Unfortunately, aerosol size distribution cannot be predicted by any existing large-scale model, nor is this a likely development in the near future. Thus it is important to test the sensitivity of climate forcing to the size distribution of sulfate aerosols. The great majority of mass derived from gas-to-particle conversion resides in the accumulation mode where its size distribution is approximately lognormal, with geometric volume mean diameters, D_{gv0}, (measured at low RH) generally between 0.2 and 0.4 μm and geometric standard deviations, σ_g, between 1.4 and 2.2 [e.g., *Whitby*, 1978; *Mészaros*, 1978; *Hoppel et al.*, 1990; *Hoppel and Frick*, 1990; *Covert and Heintzenberg*, 1993]. On the basis of these considerations, our aerosol chemistry tests use lognormal distributions with σ_g=2.0 and D_{gv0}=0.30 μm. To test the sensitivity of climate forcing to the size distribution of sulfate aerosols, we consider five aerosol types spanning a range of possibilities with D_{gv0} values of 0.15, 0.20, 0.30, 0.40, and 0.60 μm. The extreme sizes (D_{gv0} = 0.15 and 0.60 μm) are not realistic for accumulation mode sulfate but we include them to show how the sensitivity to size works. A geometric standard deviation of 1.4 is preferred in these

tests because it makes them more sensitive to changes in size (see, e.g., Figure 3 of KB93).

For a given size distribution and chemical composition, $\alpha_{sp-SO_4^=}$ and g are strong functions of wavelength. The LMD GCM provides two wavelength bands in the shortwave (0.25–0.68 μm and 0.68–4.0 μm). To derive appropriate optical properties for these wavelength bands, Mie calculations were performed for each aerosol type, at each RH, and for 24 wavebands between 0.28 and 4.0 μm. To compress the wavelength variation of optical properties into the two wavebands of the GCM, weighted averages are taken over the relevant portions of the solar power spectrum. For g, weighting is done by the product of solar power and $\alpha_{sp-SO_4^=}$. We use the solar power spectrum simulated by the Streamer radiative transfer model (J. Key, Streamer User's Guide, unpublished report, Cooperative Institute for Research in Environmental Sciences, University of Colorado, 1994) for clear sky, midlatitude, summer, bottom-of-atmosphere (BOA) conditions. We also ran one case with the top-of-atmosphere (TOA) spectrum (aerosol type K). The BOA spectrum compared to the TOA shows a loss of energy at both short wavelengths (due to Rayleigh scattering) and at longer wavelengths (due to H_2O and CO_2 absorption) such that the power becomes a little bit more concentrated in the 0.4 to 0.8 μm regions. However, these changes in solar power distribution make very little difference to the aerosol optical properties or the calculated climate forcing. The optical properties are summarized in Table 5 and in Figure 2.

4. Results and Discussion

For our base case (type A), the pattern of climate forcing is shown in Figure 3 (annually averaged geographical distribution) and Figure 4 (zonally averaged temporal distribution), while regional and temporal variations of climate forcing efficiency are explored in Table 2b and Figure 5. Sensitivity analyses, in which forcings by the various aerosol types are compared, are presented in Table 6 and Figures 6 and 7.

4.1. Geographical Pattern of the Forcing

The annually averaged direct radiative forcing of anthropogenic sulfate aerosols for our base case (aerosol type A) is estimated to be −0.47 and −0.11 W m^{-2} in the northern hemisphere (NH) and SH, respectively. Large negative radiative forcings (−1 to −3 W m^{-2}) occur over the eastern United States, Europe, Southeast Asia and, to a lesser extent, over South Africa and off the west coast of South America. The pattern of forcing (Figure 3) is very similar to the one obtained by KB93 who used similar sulfate fields and, like us, calculated direct shortwave forcing only. Small differences arise from different RH and cloudiness fields as well as differences in the RH dependence of optical properties. *Kiehl and Rodhe* [1995] used the same aerosol optical properties as KB93 but computed the forcing with sulfate abundances from *Pham et al.* [1995]. The pattern of the forcing is again similar, although the magnitude is roughly a factor of 2 larger.

Table 5. Comparison of Optical Properties among Aerosol Types

Aerosol Type	RH=30% $<\alpha_{sp-SO_4^=}>$ m^2 g^{-1}	g	$\alpha_{bsp-SO_4^=}$ m^2 g^{-1}	$<b>$	RH=80% $\alpha_{sp-SO_4^=}$ m^2 g^{-1}	g	$\alpha_{bsp-SO_4^=}$ m^2 g^{-1}	b	f(80%) $<\alpha_{sp-SO_4^=}>$	$\alpha_{bsp-SO_4^=}$
					Base Case					
A	3.12	0 60	0 368	0.118	8 86	0.70	0.704	0.079	2.84	1.91
					Hysteresis Tests					
B	3.12	0.60	0.368	0.118	8 86	0.70	0.704	0 079	2.84	1.91
C	3 12	0.60	0 368	0.118	8 86	0 70	0 704	0.079	2.84	1.91
					Particle Size Tests					
D*	1.17	0.37	0.279	0.238	4 73	0 52	0 722	0.153	4 04	2.59
E	2.02	0.48	0.351	0.174	7 16	0 61	0 752	0 105	3.54	2 14
F	3.54	0.59	0.409	0 116	10.55	0.70	0 746	0 071	2 98	1.82
G	4.44	0.64	0.430	0.097	11 91	0.74	0 735	0 062	2.68	1 71
H*	4.74	0 67	0.428	0 090	11 26	0.76	0 690	0 061	2 38	1.61
					Chemical Form Tests					
I	3.16	0.65	0.311	0.098	7 97	0 71	0 602	0 076	2 52	1 94
J	4.62	0.69	0.381	0 082	10 76	0 73	0 725	0.067	2 33	1 90
					Spectral Averaging Test					
K	3 04	0.61	0.356	0 117	8 56	0 70	0 680	0.079	2 82	1.91
Range**	±42%		±16%	±39%	±27%		±11%	±27%	±21%	±11%

Optical parameters in columns 2–10 are the scattering and backscattering efficiencies with respect to sulfate mass, $\alpha_{sp-SO_4^=}$ and $\alpha_{bsp-SO_4^=}$, the asymmetry parameter, g, the backscatter fraction, b (i.e., the ratio of $\alpha_{bsp-SO_4^=}$ to $\alpha_{sp-SO_4^=}$), for RH of 30 and 80%, and the increase in $\alpha_{sp-SO_4^=}$ and $\alpha_{bsp-SO_4^=}$ when RH is increased from 30 to 80%, f(80%). Values given for each of these parameters are weighted averages over the entire solar power spectrum (0.28–4.0 μm). The range of variation among the tested aerosol types (excluding aerosol types D and H) is given in % in the bottom row. Except that they have been averaged over all solar wavelengths, the three flagged columns, $<\alpha_{sp-SO_4^=}>$ and $<b>$ at 30% RH and the f(80%) value for $<\alpha_{sp-SO_4^=}>$, represent the key optical parameters identified by *Charlson et al.* [1991, 1992]. Note that the variability of each of these parameters is much larger than the variability of a parameter which combines all three, namely, $\alpha_{bsp-SO_4^=}$ at 80% RH. The latter parameter more accurately represents the sensitivity of climate forcing (Table 6) to aerosol type.

*Types D and H are unrealistic sizes for accumulation mode aerosols.

**Range=(Max−Min)/2/Base (excluding Types D and H).

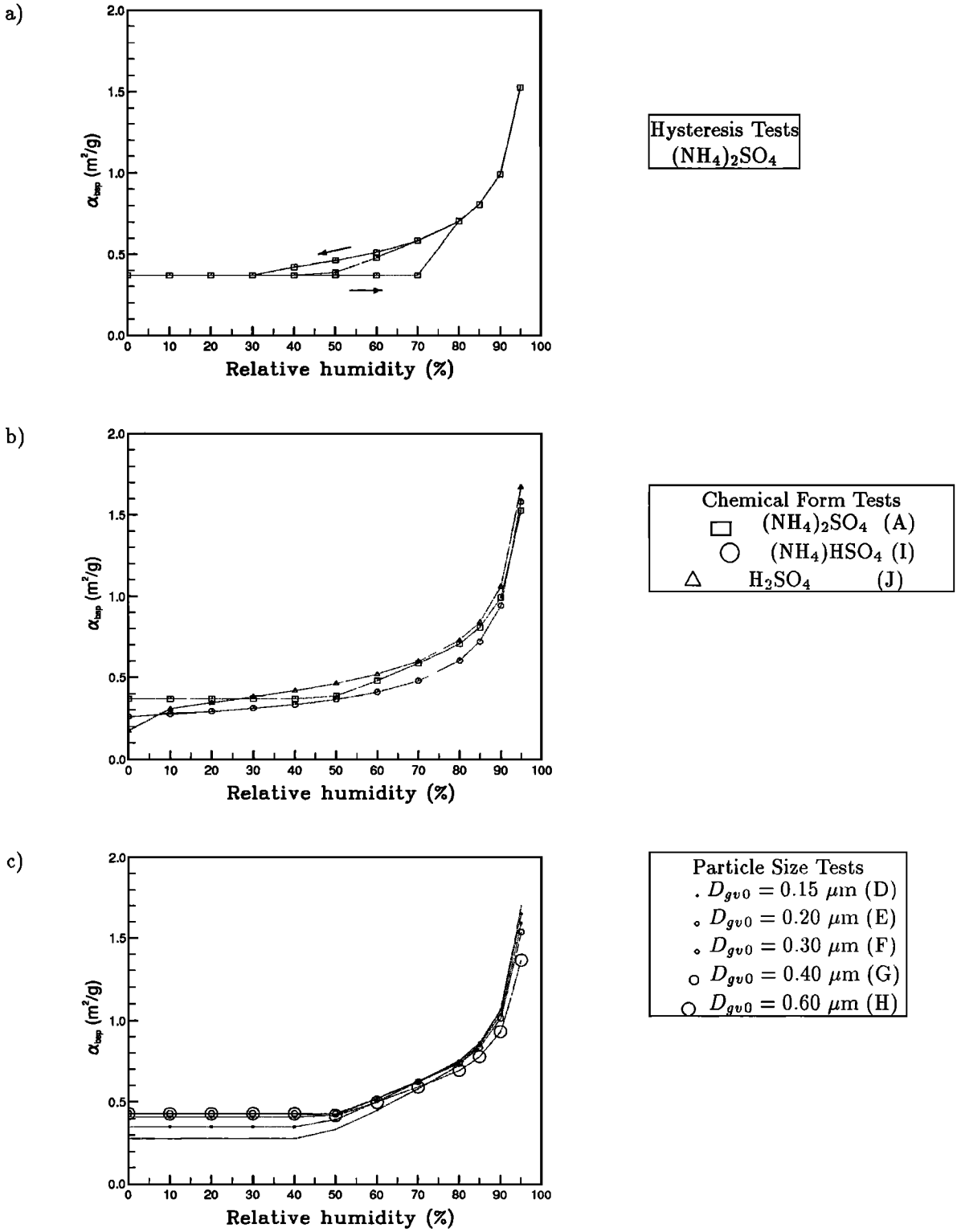

Figure 2. Mass backscattering efficiency, $\alpha_{bsp-SO_4^=}$, (meters squared per sulfate gram) for the different aerosol types as a function of relative humidity: aerosol types (a) A, B, and C, (b) A, I, and J, (c) D, E, F, G, and H.

4.2. Seasonal Variation of the Forcing

We present Hovmöller (latitude time) diagrams of the zonally averaged anthropogenic sulfate burden and sulfate forcing in Figure 4. Whereas the maximum of aerosol concentration occurs at high latitudes in January-February, the maximum of forcing is shifted toward the spring and extends into the boreal summer. This shift implies a seasonal change in climate forcing efficiency (CFE) which is shown directly in Table 2b and Fig-

Table 6. Comparison of Climate Forcings among Aerosol Types

Aerosol Type	Eastern United States, January	Eastern United States, July	Europe, January	Europe, July	NH	SH	Globe	Globe w.r.t. Base Case	Global RH Factor
				Base Case					
A	−1.26	−1.68	−1.41	−3.88	−0.47	−0.11	−0.29	0%	1.40
				Hysteresis Tests					
B	−1.06	−1.30	−1.18	−3.14	−0.40	−0.10	−0.25	−14%	1.19
C	−1.31	−1.73	−1.43	−4.14	−0.49	−0.12	−0.30	+4%	1.45
				Particle Size Tests					
D*	−0.90	−1.47	−0.98	−2.98	−0.36	−0.09	−0.23	−22%	1.71
E	−1.17	−1.77	−1.29	−3.78	−0.46	−0.12	−0.29	−1%	1.55
F	−1.49	−1.97	−1.61	−4.51	−0.54	−0.13	−0.34	+16%	1.40
G	−1.53	−1.94	−1.70	−4.64	−0.56	−0.13	−0.34	+18%	1.32
H*	−1.44	−1.71	−1.61	−4.28	−0.52	−0.12	−0.32	+10%	1.24
				Chemical Form Tests					
I	−1.09	−1.39	−1.22	−3.36	−0.39	−0.09	−0.24	−17%	1.39
J	−1.42	−1.80	−1.57	−4.38	−0.50	−0.12	−0.31	+6%	1.40
				Spectral Averaging Test					
K	−1.23	−1.65	−1.37	−3.81	−0.45	−0.11	−0.28	−3%	1.39
Range**	±25%	±20%	±18%	±21%	±17%	±18%	±17%		

Forcings are in watts per square meter. The regions are those defined in Figure 5.
*Types D and H are unrealistic sizes for accumulation mode aerosols.
**Range=(Max−Min)/2/Base (excluding Types D and H).

ure 5 for two regions of high concentration (eastern United States and Central Europe). CFE (or forcing per unit sulfate burden, with units of watts per gram $SO_4^=$) is an appropriate parameter for our study because the seasonal cycle of sulfate concentration predicted by the MOGUNTIA model appears to be somewhat inaccurate [*Langner et al.*, 1993].

As shown in Figure 5, temporal variations in CFE are not gradual and symmetrical, as would be expected from the seasonal variations in solar radiation at these midlatitude locations. Instead, CFE is strongly modulated by both day-to-day and seasonal variations in cloud cover (CC). Examining the 30-day running averages, for example, we see that the strong minimums in CC that occur in October and August, respectively, for the eastern United States and European regions during our model year produce corresponding strong maximums in CFE. Note also that the general anticorrelation of CC and solar radiation (i.e., lower CC in summer and higher in winter), tends to enhance the seasonal variation in CFE. This is especially apparent for the European region where January and July values of

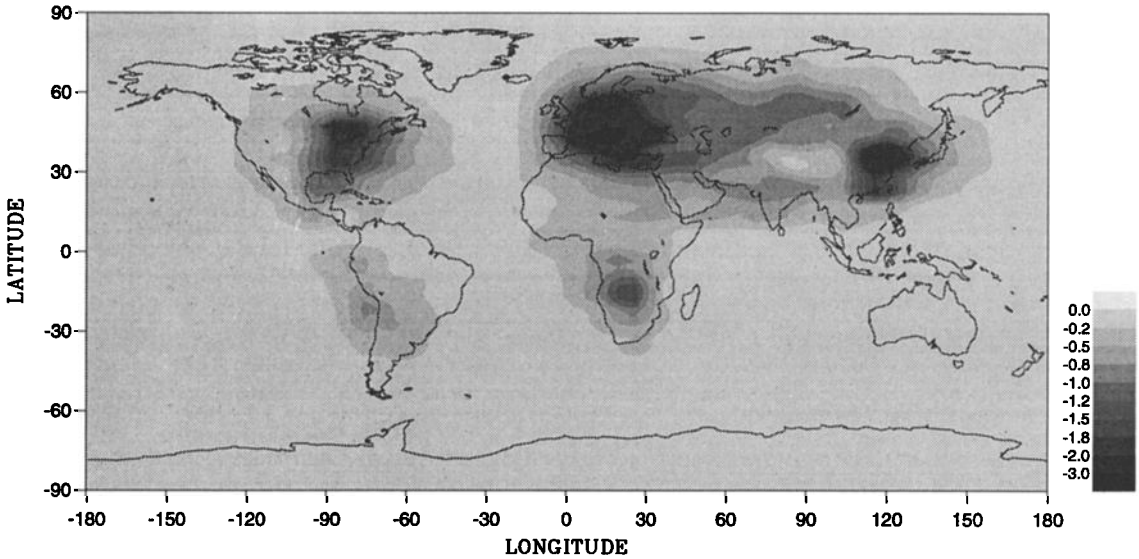

Figure 3. Annually averaged simulated loss of solar radiance (watts per square meter) at the top of the atmosphere due to the direct effect of anthropogenic sulfate aerosols (aerosol type A).

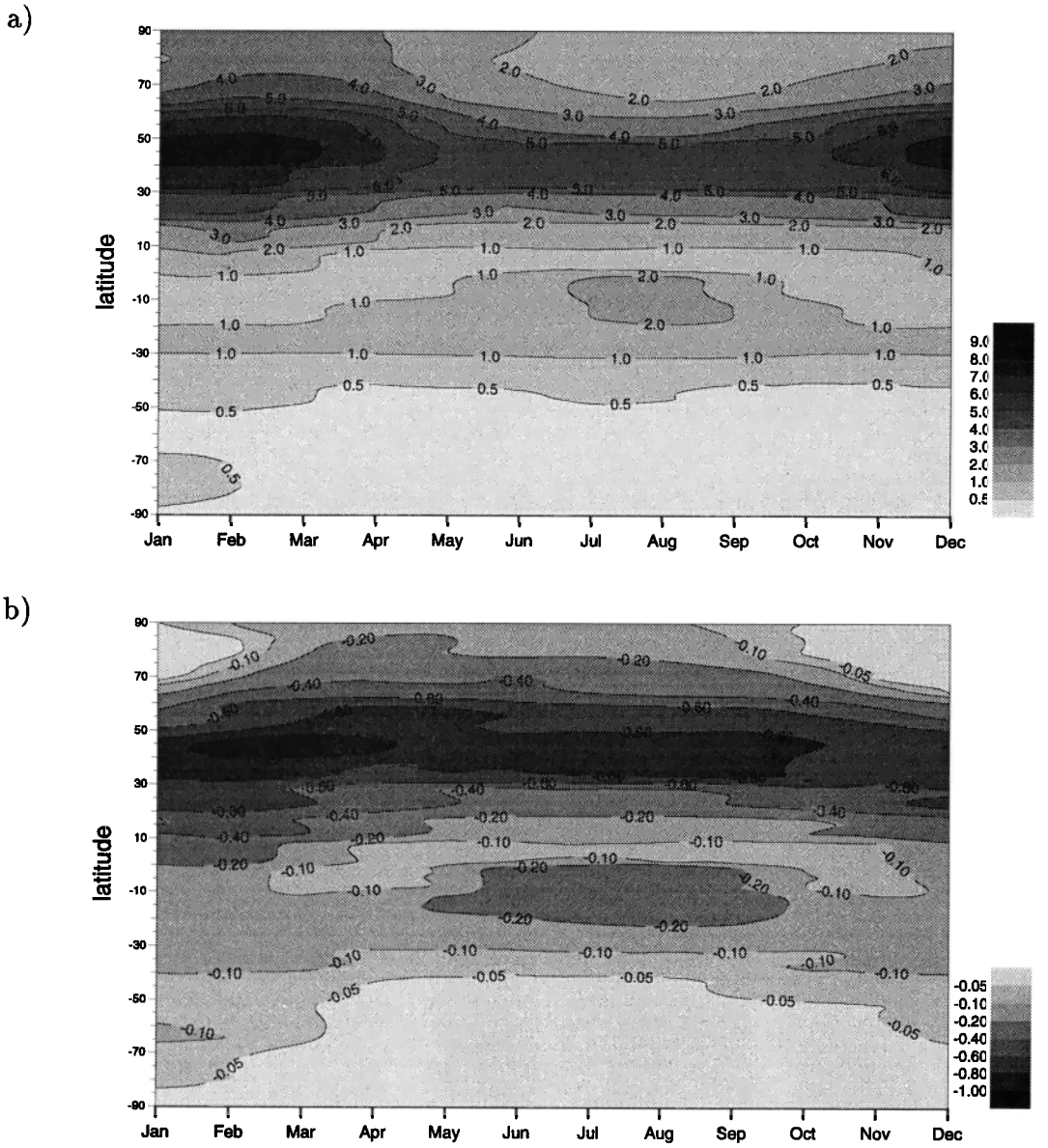

Figure 4. Hovmöller diagram of (a) the anthropogenic sulfate burden (milligrams of sulfate per square meter), and (b) the SW direct aerosol forcing (watts per square meter).

CFE differ by more than a factor of 3 (Table 2b). The large day-to-day and seasonal variations in CFE show the importance of accurately simulating the temporal variations of cloud cover and sulfate burden, including their correlations. Strong temporal variations in sulfate aerosol forcing are likely to have important implications for the response of the climate system.

4.3. Sensitivity to RH and Hysteresis

Table 6 compares climate forcing among the various aerosol types and for various spatial/temporal averages. A rather small range of variation among the aerosol types is indicated (see bottom row). It is noteworthy that this small range is not the result of global or seasonal averaging, but is also present (although slightly larger) on a regional basis.

The potential uncertainty in climate forcing due to hysteresis in the RH growth curve for ammonium sulfate aerosols can be estimated by comparing aerosol types A, B, and C. If optical properties are taken from the falling RH curve (type C) the global forcing is about 20% larger than if the rising RH curve is used (type B). This is a significant difference (not surprising given that ambient, clear sky RH is often in the hysteresis-sensitive range of 40–80%), but represents experiments based on extreme assumptions, including the assumption that all the sulfate aerosol is in the form of ammonium sulfate. Note that the base case aerosol type, based on a simple linear interpolation of the diameter growth curve between 40% RH (no growth) and 80% RH (the deliquescence point), turns out to have optical properties and climate forcing efficiencies closer to the falling RH

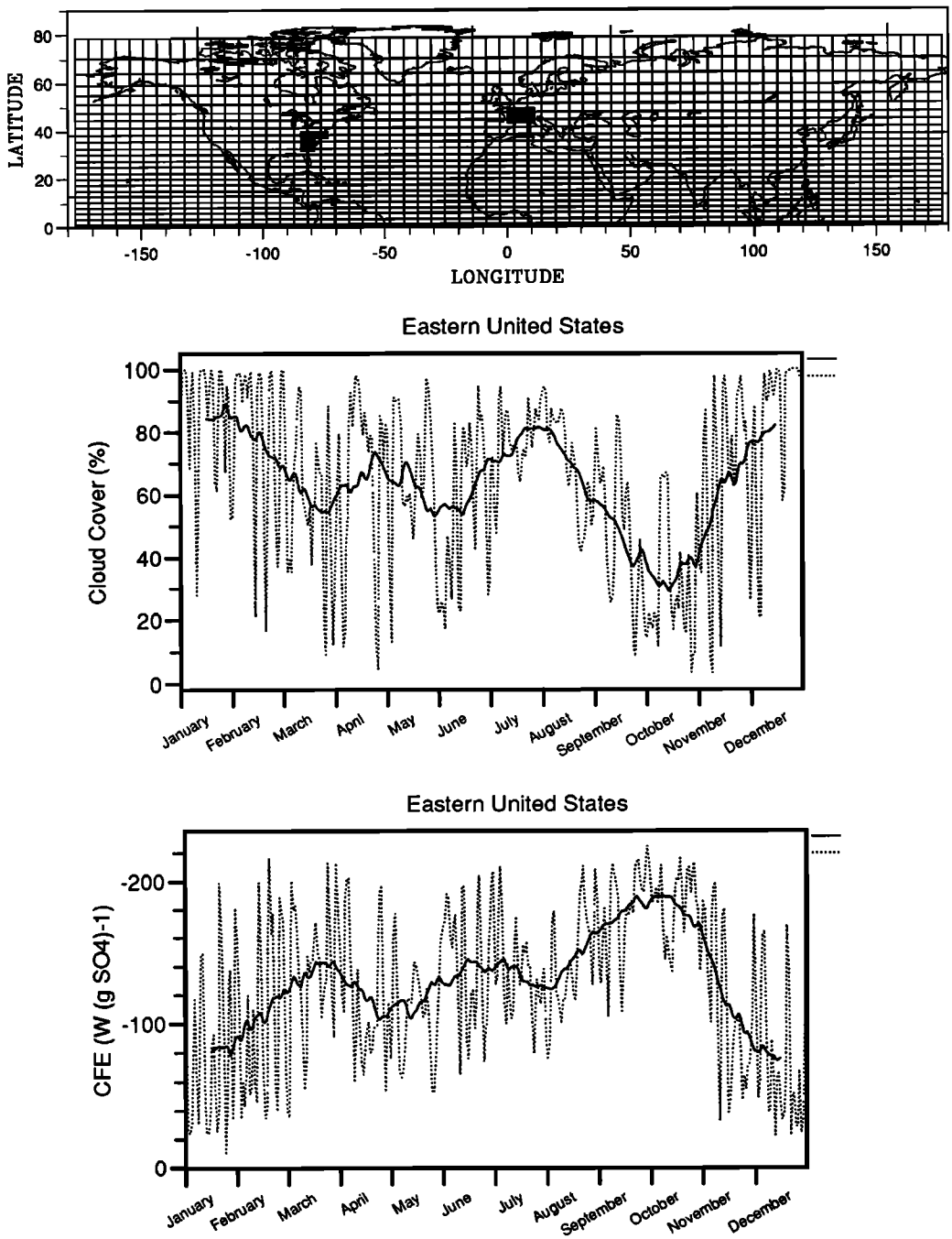

Figure 5. Seasonal variations of cloud cover (CC) and climate forcing efficiency (CFE) (watts per sulfate gram) for the two regions depicted on the map. Daily average (dotted line) and 30-day running average (solid line).

curve. This may be appropriate, since RH below 40% is rare in the boundary layer and completely neutralized sulfate aerosol is rare above the boundary layer. Thus sulfate aerosols will more frequently be in the hydrated than the crystallized state at atmospheric humidities between 40 and 80%.

4.4. Sensitivity to Aerosol Chemistry

The three chemical forms studied here (aerosol types A, I, and J) are compared in Figure 6 in terms of climate forcing efficiency as well as key hydration dependent properties. As explained above, aerosol type A is believed to be the most realistic type for ammonium sulfate. However, considering aerosol types B or C instead of type A would not alter our conclusions. We find that H_2SO_4 is the most effective at backscattering sunlight, $(NH_4)HSO_4$ is the least effective, and the differences are rather small (+6% and −17%, respectively), due to a number of compensating factors. Sulfuric acid is extremely hygroscopic such that it draws considerable water vapor into the particulate phase even at low RH, thereby increasing the amount of scattering and

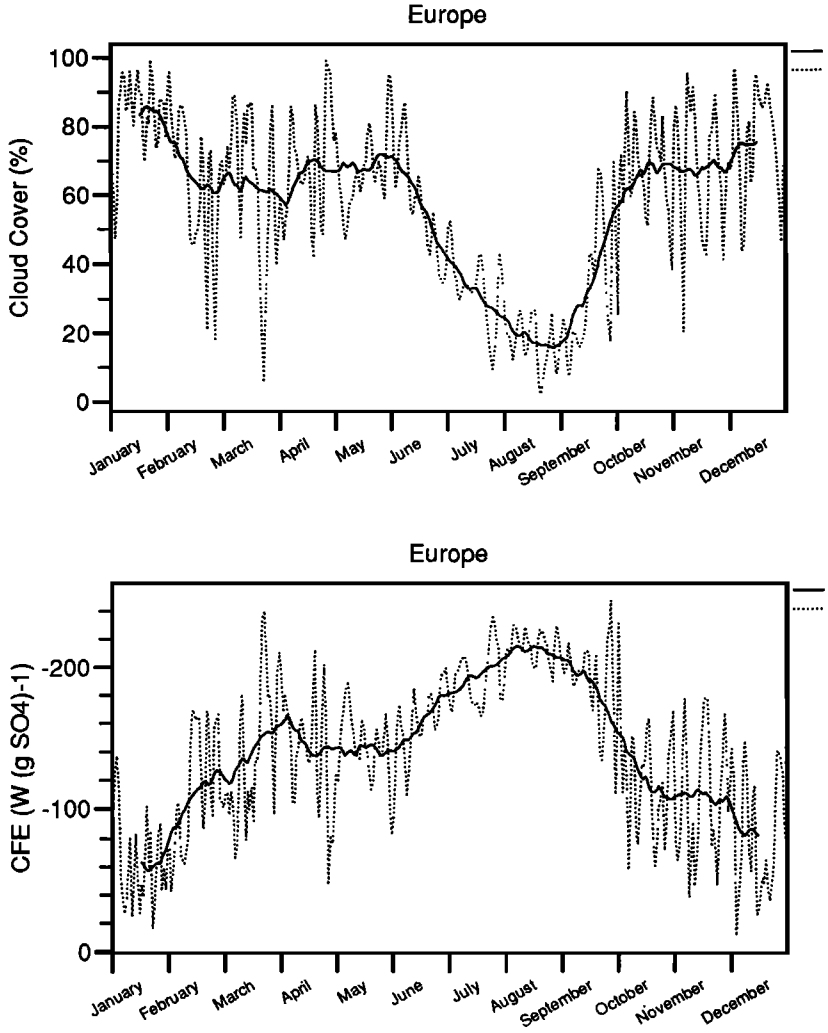

Fig. 5. (continued)

backscattering per unit mass of sulfate. In the presence of ammonia gas, acidic sulfate will become partially or fully neutralized by drawing the available ammonia into the particulate phase (up to a molar ratio of two). The resulting increase in particulate mass due to ammonia will be offset by a decrease in hygroscopicity (especially at lower RH) and therefore in water mass. In general, sulfuric acid tends to attract the most additional mass into the particulate phase (i.e., $C_{SO_4^=}$ is the smallest, Figure 6), but the resulting particles have the lowest refractive index (Figure 6) and the lowest ratio of backscattering to total scattering (Table 5). KB93 found a 5% difference in forcing between sulfuric acid and ammonium sulfate, similar to our result. However, our study shows that the intermediate chemical form, ammonium bisulfate, turns out to have the minimum climate forcing efficiency. Some observations [e.g., *Covert*, 1988] indicate that ammonium bisulfate may be a common molecular form of sulfate aerosols, at least in the lower marine atmosphere.

4.5. Sensitivity to Particle Size

Comparing types D to H in Table 6, one can note that the climate forcing (for the same sulfate mass distribution) increases as particle size increases from 0.15 μm to 0.30 μm (dry geometric volume mean diameter, D_{gv0}), is almost flat between 0.3 and 0.4 μm, and decreases between 0.4 and 0.6 μm. Because climate forcing efficiency goes through a maximum within the accumulation mode, it is not terribly sensitive to size changes within the accumulation mode. As stated in the previous section, $0.2 < D_{gv0} < 0.4$ μm represents the range of measured accumulation mode sizes (we include tests D and H simply to illustrate size dependent tendencies). Across this range, climate forcing varies by only $\pm 9\%$. The reasons climate forcing efficiency goes through a maximum between 0.3 and 0.4 μm (as illustrated in Figure 7) can be seen by comparing the optical properties for types D to H in Table 5. Low RH scattering efficiency, $\alpha_{sp-SO_4^=}$, is greatest at the largest size of 0.6 μm, while low RH backscattering efficiency, $\alpha_{bsp-SO_4^=}$, peaks somewhere between 0.4 and 0.6 μm. This shows that most of the increase in total scatter between 0.4 μm and 0.6 μm takes place in the forward hemisphere. Turning to the high RH case (which better represents average conditions in the lower atmosphere), $\alpha_{sp-SO_4^=}$ is seen to peak at 0.4 μm. This shows that hydration has brought the 0.6 μm aerosol over the peak in the scat-

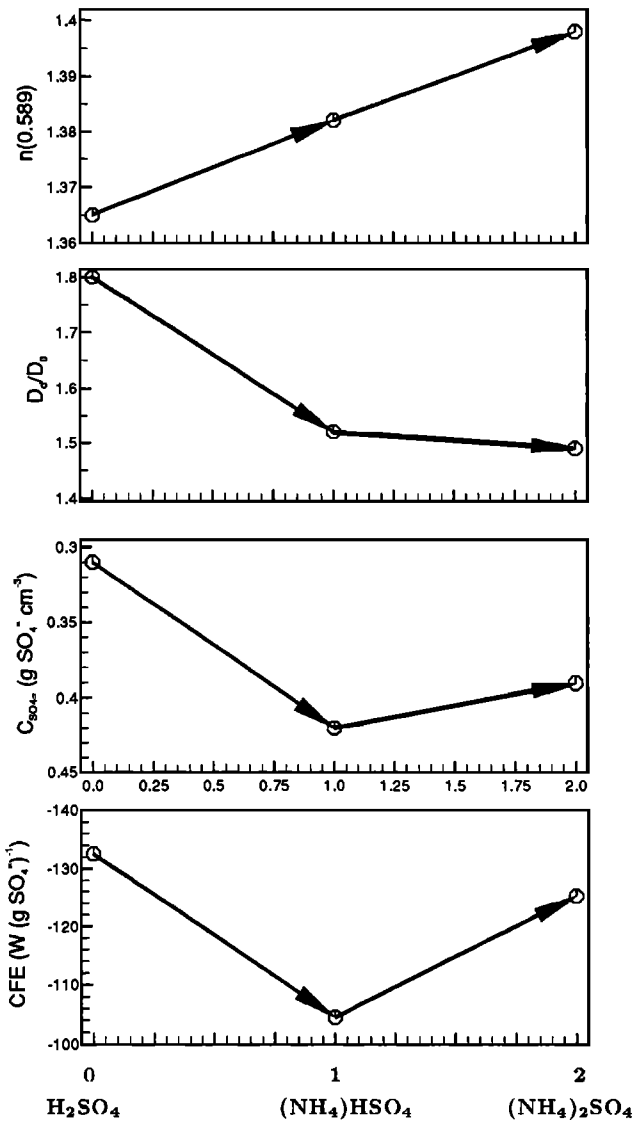

Figure 6. Sensitivity to chemical form. Hydration dependent factors affecting optical properties and thus climate forcing efficiency (CFE) are refractive index, $n(0.589)$, diameter growth, D_d/D_0, and the liquid-phase sulfate concentration, $C_{SO_4^=}$. Values for these factors are shown at 80% RH and are plotted for each of the three chemical forms. The arrows indicate the effect on the different quantities of changing the ammonium-to-sulfate ratio from 0 to 1 and 1 to 2. $C_{SO_4^=}$ is plotted with an inverted y axis, since lower values correspond to higher CFE. For reference, bottom panel shows CFE with an inverted y axis.

tering efficiency curve. For $\alpha_{bsp-SO_4^=}$ at 80% RH, the peak occurs at 0.2 μm. This shows that the change in backscatter ratio (or, equivalently, asymmetry parameter) with RH is indeed a significant factor. The fact that climate forcing peaks somewhere between the peaks in $\alpha_{sp-SO_4^=}(80\%)$ and $\alpha_{bsp-SO_4^=}(80\%)$ indicates that forward hemisphere scattering does make an important contribution to the backscattering of sunlight to space [*Wiscombe and Grams*, 1976].

Our study reveals a somewhat different dependence of climate forcing on D_{gv0} than that found by KB93 (see Figure 7). We ascribe this to the fact that KB93 incorporated the size variation of low RH scattering efficiency but took $f(\mathrm{RH})$ as an invariant function. Our results indicate that $f(\mathrm{RH})$ decreases rather rapidly with increasing size throughout the accumulation mode (see $f(80\%)$ for $\alpha_{sp-SO_4^=}$ and $\alpha_{bsp-SO_4^=}$ in Table 5 and the RH factor in Table 6), which will tend to offset partially the increase in low RH scattering efficiency. Thus including the size dependence of $f(\mathrm{RH})$ has the effect, shown in Figure 7, of significantly reducing the size dependence of climate forcing and of shifting the peak forcing to smaller sizes.

4.6. Relative Humidity Factor

We can define an effective RH factor as the ratio between climate forcing by the hydrated aerosol (using RH predicted by the GCM) and climate forcing computed for a constant RH value of 30%. This effective RH factor will depend on the hydration properties of each aerosol type. As shown in Table 6, it varies between 1.19 and 1.71. It is significantly higher for the falling RH curve aerosol (1.45) than for the rising RH curve aerosol (1.19). The RH factor decreases sharply with particle size (see types D–H), a result consistent with the backscattering efficiencies shown in Figure 2c, the $f(80\%)$ values for both backscatter and total scatter shown in Table 5, and with a previous modeling study of this effect [*Hegg et al.*, 1993]. If we take aerosol type A as a reasonably accurate representation of the hydration behavior of ammonium sulfate (a point discussed in section 4.3), Table 6 indicates little chemical dependence to the effective RH factor despite the fact that H_2SO_4 is considerably more hygroscopic than the other forms. This occurs because the low RH value (which produces the denominator in our calculated ratio) is set

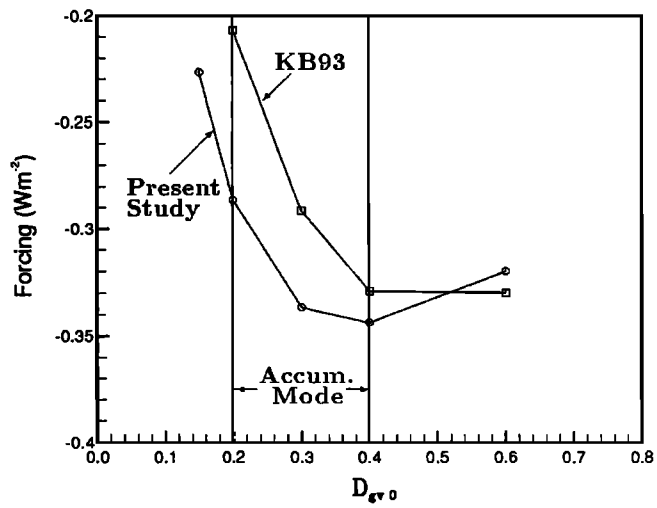

Figure 7. Sensitivity to aerosol size. Globally-averaged aerosol forcing (watts per square meter) as a function of the geometric volume mean diameter, D_{gv0} (in micrometers), and for σ_g=1.4. The vertical lines show realistic limits for accumulation mode D_{gv0}.

at 30%, where sulfuric acid is already quite hydrated. As shown in Figure 2b, the ratio of backscattering efficiency among the three chemical forms does not change significantly above 30% RH. Note that this finding has some significance for studies of the RH dependence of optical properties: for acidic aerosols, measured growth factors can be quite sensitive to the RH value chosen for the low RH reference condition.

4.7. Cloud-free Forcing

To study how clouds affect aerosol scattering in the model, we have also computed the aerosol radiative forcing in the absence of clouds. Denoting ΔF and ΔF_{clear} as the calculated forcing with and without clouds, respectively, we define a cloud factor (Table 2) as the ratio $\Delta F/\Delta F_{clear}$. For global averages of ΔF and ΔF_{clear}, this ratio is 0.61 for our model compared to 0.64 and 0.74 in the simulations of KB93 (B. Briegleb, personal communication, 1994) and *Chuang et al.* [1994]. These differences are not easy to interpret because they depend on the amount of cloudiness, the relative vertical position of clouds and aerosols, and the way cloud overlap is treated in the model [*Morcrette and Fouquart*, 1986; *Briegleb*, 1992].

The cloudy-to-cloudless forcing ratios in all three of the cited models imply that aerosol forcing (due to the direct effect) is nonzero in cloud-covered regions. This can be shown by a simple bulk parameterization (B. Briegleb, personal communication, 1994) in which ΔF is assumed to be the sum of contributions from cloud-free and cloud-covered regions:

$$\Delta F = \Delta F_{clear}\,(1 - \mathrm{CC}) + \Delta F_{cloud}\,\mathrm{CC} \qquad (6)$$

Here CC is the fractional cloud cover (determined by the GCM). Since the other terms are known, (6) can be solved for ΔF_{cloud}, the average direct forcing in cloudy regions. For the global annual average and the base case aerosol, ΔF=−0.29 W m^{-2}, ΔF_{clear}=−0.48 W m^{-2}, and CC = 0.526. Thus according to (6), we have ΔF_{cloud} = −0.12 W m^{-2}, $\Delta F_{cloud}/\Delta F_{clear}$=0.25 (the aerosol is 25% as efficient at backscattering sunlight in the cloudy as compared to the clear regions), and ΔF_{cloud} CC/ΔF=0.22 (22% of the direct aerosol forcing occurs in cloud-covered regions). Using the same bulk parameterization, forcing in cloudy regions accounts for 40% of the direct forcing in the KB93 study (B. Briegleb, personal communication, 1994). Again, this difference is hard to interpret. The calculation, it should be noted, is very sensitive to the method of estimating CC from the three-dimensional distribution of cloudiness predicted by the GCM.

Direct forcing in cloud-covered regions was explored for our model by removing the in-cloud aerosol scattering. This resulted in a small decrease in the total forcing ΔF of about 7% and an equivalent decrease in the cloudy-to-cloudless forcing ratio, implying that aerosols above the cloud layer are responsible for most of the direct effect in cloudy regions. (Aerosols underlying a cloud layer must have a much smaller effect on TOA fluxes because they only interact with a part of the incoming solar radiation and because the upward reflected radiation is once again scattered by the clouds.)

4.8. Bottom-of-Atmosphere Forcing

The aerosol radiative forcing at the BOA is 2.9% smaller than at the TOA. Since the aerosols considered here are nonabsorbing (i.e., purely scattering), the reason for this difference must be sought in the combination of aerosol, air molecule, and cloud effects. Indeed the forcing at the BOA and at the TOA in the absence of clouds, when only Rayleigh and aerosol scattering and molecular absorption are considered, differ only by 1.5%. Radiation backscattered to space by aerosols is lost for cloud and molecular absorption so that aerosols (even purely scattering) modify the shortwave fluxes somewhat more at the TOA than at the BOA.

5. Conclusion

An assessment of the sensitivity of direct climate forcing by anthropogenic sulfate aerosols to aerosol size and chemistry has been performed. Our investigation takes the predicted global distribution of anthropogenic sulfate mass from a chemical/transport model as the basis for calculating shortwave aerosol radiative effects within a GCM. We begin by examining the relationships between aerosol climate forcing and such climatic parameters as RH, cloud cover, underlying surface, and season of year, comparing our results, where possible, to those of previous investigators (C91; KB93). Our study focuses on sulfate optical properties, which are the required connection between sulfate mass concentrations and radiative perturbations. These optical properties depend fundamentally on aerosol size and chemistry such that specifying these optical properties is equivalent to specifying a physical/chemical model of the sulfate aerosol. Our physical/chemical model reduces, in essence, to two following assumptions: (1) anthropogenic sulfate mass resides in accumulation mode sized particles and (2) anthropogenic sulfate interacts only with ammonia gas and/or water vapor. This model is simple but plausible; most important, because extensive hydration data exists for the ammonium/sulfate/water system, these assumptions permit a self-consistent study of the influence of particle size and chemical form on climate forcing efficiency. The major implications of this study are as follows:

1. Within our assumptions, the optical properties of sulfate aerosol are well constrained; variations in size and chemical form introduce only a ±20% uncertainty in direct climate forcing. This is larger than the ±10% uncertainty estimated by KB93, but still small enough to give hope that accurate estimates of direct forcing by anthropogenic aerosols can be obtained with the existing generation of global-scale models. It also suggests that efforts to predict the details of accumulation mode size distributions may be much less important to the direct forcing question than efforts (1) to predict the fraction of anthropogenic sulfate that forms on

coarse mode particles (where it contributes very little to climate forcing) and (2) to predict the extent and the effects of sulfate interactions with other accumulation mode aerosol components. Regarding the former issue, it is clearly vital that the coarse and accumulation modes be separately modeled and analyzed in measurement campaigns. Regarding the latter, a particularly important (and difficult) problem is to understand the extent to which the formation of acidic sulfate aerosol causes volatilization of preexisting accumulation mode components such as nitrate, chloride, or organics.

2. Where *Charlson et al.* [1991] identified three optical parameters which need to be predicted in order to predict direct climate forcing by anthropogenic sulfate, we find substantial interdependence and compensation among these parameters such that a simple summation of their individual uncertainties [*Charlson et al.*, 1992; *Schlesinger et al.*, 1992] greatly overestimates the net uncertainty for climate forcing. These three parameters, the sulfate scattering efficiency at low RH, the ratio of backscatter to total scatter, and the increase in scattering from low RH to typical tropospheric values like 80%, may be combined into a single parameter, the backscattering efficiency at 80% RH. This parameter exhibits variability quite comparable to that of climate forcing in our tests. In principle, this is a quantity which can be measured as well as predicted from independent measurements of aerosol size and chemistry. This suggests that high RH backscattering efficiency is a logical focus for research on local aerosol optical properties as they relate to direct climate forcing. Conversely, studies which focus exclusively on low RH total scattering efficiency (or exclusively on backscatter ratio or $f(\mathrm{RH})$), are likely to misrepresent the uncertainty of climate forcing estimates.

3. The direct effect in cloud-covered regions (that is, the enhancement of planetary albedo by sulfate aerosols located above a cloud layer) cannot be ignored. In both our study and that of KB93, this accounts for a significant fraction of sulfate aerosol direct forcing. This effect, which arises because low clouds cover such a large portion of the Earth and because the chemical/transport models predict substantial anthropogenic sulfate in the free troposphere, will be much harder to validate than the clear sky effect.

Acknowledgments. Thanks are due to Ulf Hansson who provided the data from the MOGUNTIA model, Steve Marshall who developed the Mie computation scheme, Bruce Briegleb for useful conversations, and Henning Rodhe for encouragement. Both authors would like to thank the Department of Meteorology, Stockholm University, for its hospitality. Olivier Boucher also acknowledges the Swedish Institute for support. Tad Anderson acknowledges support from the U.S. National Science Foundation International Program, the U.S. Department of Energy/National Institute for Global Environment Change through its Western Regional Center, and the University of Washington Joint Institute for the Study of the Atmosphere and Ocean (JISAO contribution 295). Computer time for numerical experiments was provided by IDRIS (Institut de Développement et des Ressources en Informatique Scientifique), Paris.

References

Atwater, M. A., Planetary albedo changes due to aerosols, *Science*, *170*, 64–66, 1970.

Bohren, C. F., and D. R. Huffman, *Absorption and Scattering of Light by Small Particles*, John Wiley, New York, 1983.

Bolin, B., and R. J. Charlson, On the role of the tropospheric sulfur cycle in the shortwave radiative climate of the Earth, *Ambio*, *5*, 47–54, 1976.

Briegleb, B. P., Delta-Eddington approximation for solar radiation in the NCAR Community Climate model, *J. Geophys. Res.*, *97*, 7603–7612, 1992.

Charlson, R. J., and M. J. Pilat, Climate: The influence of aerosols, *J. Appl. Meteorol.*, *8*, 1001–1002, 1969.

Charlson, R. J., W. M. Porch, A. P. Waggoner, and N. C. Ahlquist, Background aerosol light scattering characteristics: Nephelometric observations at Mauna Loa Observatory compared with results at other remote locations, *Tellus*, *26*, 345–360, 1974.

Charlson, R. J., D. S. Covert, and T. V. Larson, Observation of the effect of humidity on light scattering by aerosols, in *Hygroscopic Aerosols*, edited by L. H. Ruhnke and A. Deepak, pp. 35–44, A. Deepak, Hampton, Va., 1984.

Charlson, R. J., J. Langner, H. Rodhe, C. B. Levoy, and S. G. Warren, Perturbation of the northern hemisphere radiative balance by backscattering from anthropogenic sulfate aerosols, *Tellus*, *43AB*, 152–163, 1991.

Charlson, R. J., S. E. Schwartz, J. M. Hales, R. D. Cess, J. A. Coakley, J. E. Hansen, and D. J. Hofmann, Climate forcing by anthropogenic aerosols, *Science*, *255*, 423–430, 1992.

Chuang, C. C., J. E. Penner, K. E. Taylor, and J. J. Walton, Climate effects of anthropogenic sulfate: Simulations from a coupled chemistry/climate model, in *AMS Conference on Atmospheric Chemistry*, pp. 170–174, Nashville, Tenne., Jan. 23–28, 1994.

Coakley, J. A., R. D. Cess, and F. B. Yurevich, The effects of tropospheric aerosols on the Earth's radiation budget: A parameterization for climate models, *J. Atmos. Sci.*, *40*, 116–138, 1983.

Covert, D. S., North Pacific marine background aerosol: Average ammonium to sulfate molar ratio equals 1, *J. Geophys. Res.*, *93*, 8455–8458, 1988.

Covert, D. S., and J. Heintzenberg, Size distributions and chemical properties of aerosol at Ny Ålesund, Svalbard, *Atmos. Environ.*, *27A*, 2989–2993, 1993.

Covert, D. S., R. J. Charlson, and N. C. Ahlquist, A study of the relationship of chemical composition and humidity to light scattering by aerosols, *J. Appl. Meteorol.*, *11*, 968–976, 1972.

Fouquart, Y., and B. Bonnel, Computations of solar heating of the Earth's atmosphere: A new parameterization, *Beitr. Phys. Atmos.*, *53*, 35–62, 1980.

Hänel, G., and M. Lehmann, Equilibrium size of aerosol particles and relative humidity: New experimental data from various aerosol types and their treatment for cloud physics application, *Contrib. Atmos. Phys.*, *54*, 57–71, 1981.

Hegg, D. A., T. Larson, and P.-F. Yuen, A theoretical study of the effect of relative humidity on light scattering by tropospheric aerosols, *J. Geophys. Res.*, *98*, 18,435–18,439, 1993.

Hoppel, W. A., and G. M. Frick, Submicron aerosol size distributions measured over the Tropical and South Pacific, *Atmos. Environ.*, *24A*, 645–659, 1990.

Hoppel, W. A., J. W. Fitzgerald, G. M. Frick, R. E. Larson, and E. J. Mack, Aerosol size distributions and optical properties found in the marine boundary layer over the Atlantic Ocean, *J. Geophys. Res.*, *95*, 3659–3686, 1990.

Kent, G. S., G. K. Yue, U. O. Farrukh, and A. Deepak, Modeling atmospheric aerosol backscatter at CO_2 laser wavelengths, 1, Aerosol properties, modeling techniques, and associated problems, *Appl. Opt.*, *22*, 1655–1665, 1983.

Kiehl, J. T., and B. P. Briegleb, The relative roles of sulfate aerosols and greenhouse gases in climate forcing, *Science*, *260*, 311–314, 1993.

Kiehl, J. T., and H. Rodhe, Modeling geographical and seasonal forcing due to aerosols, in *Aerosol Forcing of Climate*, edited by R. J. Charlson and J. Heintzenberg, pp. 281–296, John Wiley, New York, 1995.

Langner, J., and H. Rodhe, A global three-dimensional model of the tropospheric sulfur cycle, *J. Atmos. Chem.*, *13*, 225–263, 1991.

Langner, J., H. Rodhe, P. J. Crutzen, and P. Zimmermann, Anthropogenic influence of the distribution of tropospheric sulphate aerosol, *Nature*, *359*, 712–716, 1992.

Langner, J., et al.: The global atmospheric sulfur cycle: An evaluation of model predictions and observations, *Rep. CM-81*, 28 pp., Dep. of Meteorol., Stockholm Univ., 1993.

Le Treut, H., and Z. X. Li, Sensitivity of an atmospheric general circulation model to prescribed SST changes: Feedback effects associated with the simulation of cloud optical properties, *Clim. Dyn.*, *5*, 175–187, 1991.

McCormick, R. A., and H. Ludwig, Climate modification by atmospheric aerosols, *Science*, *156*, 1358–1359, 1967.

Mészaros, E., On the concentration and size distribution of atmospheric sulfate particles under rural conditions, *Atmos. Environ.*, *12*, 2425–2428, 1978.

Mokhov, I. I., and M. E. Schlesinger, Analysis of global cloudiness, 2, Comparison of ground-based and satellite-based cloud climatologies, *J. Geophys. Res.*, *99*, 17,045–17,065, 1994.

Morcrette, J.-J., Description of the radiative scheme in the ECMWF model, *Tech. Rep. 165*, 26 pp., Euro. Cent. for Medium-Range Weather Forecasts, Reading, England, 1989.

Morcrette, J.-J., Radiation and cloud radiative properties in the European Centre for Medium Range Weather Forecasts forecasting system, *J. Geophys. Res.*, *96*, 9121–9132, 1991.

Morcrette, J.-J., and Y. Fouquart, The overlapping of cloud layers in shortwave radiation parameterizations, *J. Atmos. Sci.*, *43*, 321–328, 1986.

Palmer, K. D., and D. Williams, Optical constants of sulfuric acid: Applications to the clouds of Venus?, *Appl. Opt.*, *14*, 208–219, 1975.

Pham, M., J.-F. Müller, G. Brasseur, C. Granier, and G. Mégie, A three-dimensional study of the tropospheric sulfur cycle, *J. Geophys. Res.*, in press, 1995.

Ramanathan, V., R. D. Cess, E. F. Harrison, P. Minnis, B. R. Barkstrom, E. Ahmad, and D. Hartmann, Cloud-radiative forcing and climate: Results from the Earth Radiation Budget Experiment, *Science*, *243*, 57–62, 1989.

Rasool, S. I., and S. H. Schneider, Atmospheric carbon dioxide and aerosols: Effects of large increases on global climate, *Science*, *173*, 138–141, 1971.

Rood, M. J., M. A. Shaw, T. V. Larson, and D. S. Covert, Ubiquitous nature of ambient metastable aerosol, *Nature*, *357*, 537–539, 1989.

Sadourny, R., and K. Laval, January and July performance of the LMD general circulation model, in *New Perspectives in Climate Modelling*, pp. 173–198, edited by A. Berger and C. Nicolis, Elsevier, New York, 1984.

Schlesinger, M. E., X. Jiang, and R. J. Charlson, Implication of anthropogenic atmospheric sulphate for the sensitivity of the climate system, in *Climate Change and Energy Policy*, pp. 75–108, edited by L. Rosen and R. Glasser, Am. Inst. of Phys., New York, 1992.

Shaw, M. A., and M. J. Rood, Measurement of the crystallization humidities of ambient aerosol particles, *Atmos. Environ.*, *24A*, 1837–1841, 1990.

Stelson, A. W., Urban aerosol refractive index prediction by partial molar refraction approach, *Environ. Sci. Technol.*, *24*, 1676–1679, 1990.

Tang, I. N., and H. R. Munkelwitz, Water activities, densities, and refractive indices of aqueous sulfate and nitrate droplets of atmospheric importance, *J. Geophys. Res.*, *99*, 18,801–18,808, 1994.

Taylor, K. E., and J. E. Penner, Response of the climate system to atmospheric aerosols and greenhouse gases, *Nature*, *369*, 734–737, 1994.

Toon, O. B., and J. B. Pollack, A global average model of atmospheric aerosols for radiative transfer calculations, *J. Appl. Meteorol.*, *15*, 225–246, 1976.

Twomey, S., Pollution and the planetary albedo, *Atmos. Environ.*, *8*, 1251–1256, 1974.

Twomey, S., The influence of pollution on the shortwave albedo of clouds, *J. Atmos. Sci.*, *34*, 1149–1152, 1977.

Twomey, S. A., M. Piepgrass, and T. Wolfe, An assessment of the impact of pollution on global cloud albedo, *Tellus*, *36B*, 356–366, 1984.

Weast, R. C., Physical constants of inorganic compounds, in *CRC Handbook of Chemistry and Physics: 68th edition*, pp. B67–146, edited by R. C. Weast, CRC Press, Boca Raton, Fla., 1987.

Whitby, K. T., The physical characteristics of sulfur aerosols, *Atmos. Environ.*, *12*, 135–159, 1978.

White, W. H., The chemical composition of fine particles, in *Visibility: Existing and Historical Conditions – Causes and Effects*, pp. 90–94, edited by J. C. Trijonis, U. S. Nat. Acid Precipitation Assess. Prog., Washington, D. C., 1990.

Wiscombe, W. J., and G. W. Grams, The backscattered fraction in two-stream approximations, *J. Atmos. Sci.*, *33*, 2440–2451, 1976.

Zimmermann, P. H., *Ein dreidimensionales numerisches Transportmodell für atmosphärische Spürenstoffe*, Ph.D. thesis, University of Mainz, Germany, 160 pp., 1984.

Zimmermann, P. H., MOGUNTIA: A handy global tracer model, in *Proceedings of the sixteenth NATO/CCMS International Technical Meeting on Air Pollution Modeling and Its Application*, pp. 593–608, Lindau, Germany, D. Reidel, Norwell, Mass., 1987.

T. L. Anderson, Department of Atmospheric Sciences, University of Washington, Box 351640, Seattle, WA 98195–1640. (e-mail: tadand@atmos.washington.edu)

O. Boucher, Laboratoire de Météorologie Dynamique du CNRS, Ecole Normale Supérieure, 24 rue Lhomond, 75231 Paris Cedex 05, France. (e-mail: boucher@lmd.ens.fr)

(Received December 12 ,1994; revised July 17, 1995; accepted July 31, 1995.)